Science Advances
AAAS

Supplementary Materials for

An extra-clock ultradian brain oscillator sustains circadian timekeeping

Min Tang *et al.*

Corresponding author: Dong-Gen Luo, dgluo@pku.edu.cn

Sci. Adv. **8**, eabo5506 (2022)
DOI: 10.1126/sciadv.abo5506

The PDF file includes:

Other Supplementary Material for this manuscript includes the following:

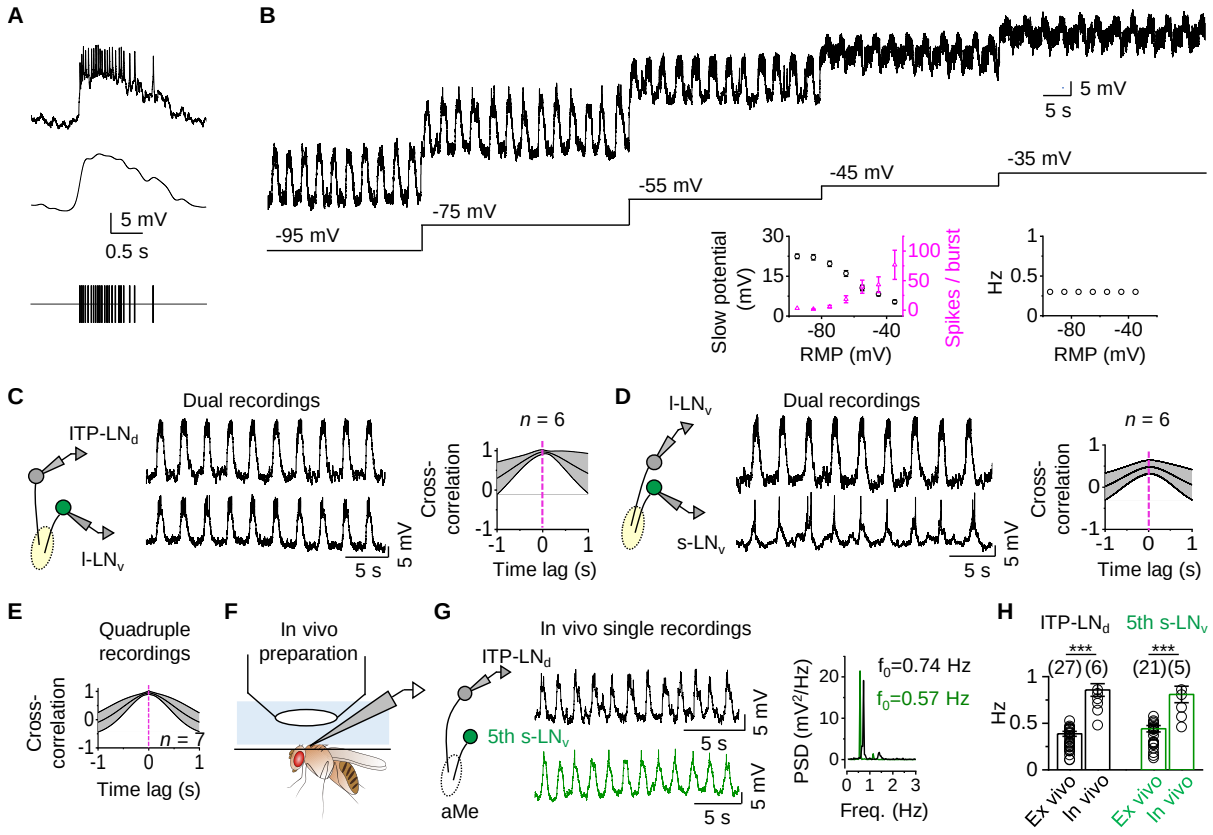

Fig. S1.

Synchronous bursting in clock neurons. (**A**) Representative burst of ITP-LN$_d$ (top); slow rhythmic depolarization, low-pass filtered at 20 Hz (middle); spike train within burst, high-pass filtered at 100 Hz (bottom). (**B**) Top, representative current-clamp recordings of ITP-LN$_d$ at holding membrane potentials indicated; bottom, plotting combined amplitude of slow depolarization and number of intra-burst action potentials (left) and the frequency of slow rhythmic depolarization (right) against holding potentials. (**C**) Left, schematic of dual recordings from ITP-LN$_d$ and l-LN$_v$ ipsilateral pair; middle, representative dual recordings; right, combined cross-correlation analysis. (**D**) Left, schematic of dual recordings from s-LN$_v$ and l-LN$_v$ ipsilateral pairs; middle, representative dual recordings; right, combined cross-correlation analysis. (**E**) Combined cross-correlation analysis of quadruple recordings from 7 ex vivo preparations. (**F**) Schematic of patch-clamp recordings in live flies. (**G**) Left, schematic of in vivo single recordings (left), representative single recordings (middle), power spectral analysis (right). (**H**) Combined data of in vivo and ex vivo recordings. ***$P < 0.001$ by unpaired two-tailed Student's *t*-test. PSD, power spectral density. Combined data are represented as means ± SEM.

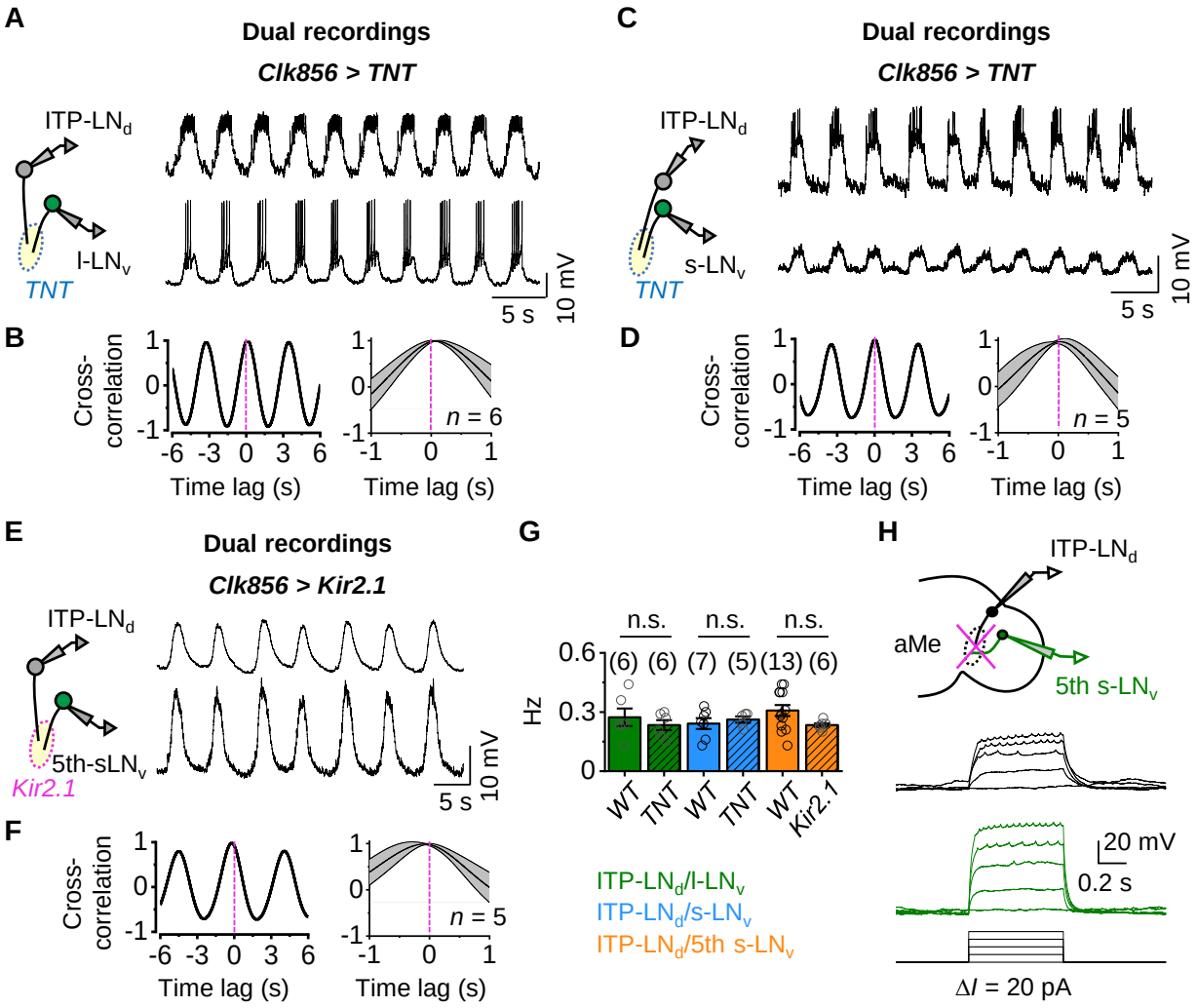

Fig. S2.

Extra-clock burst inputs. (**A**) Representative dual recordings of ipsilateral ITP-LN$_d$ and l-LN$_v$ pair in *Clk856-TNT* flies. (**B**) Cross-correlation analysis of recordings in (**A**) (left), combined data (right). (**C**) Representative recordings of ITP-LN$_d$ and s-LN$_v$ ipsilateral pair in *Clk856-TNT* flies. (**D**) Cross-correlation analysis of recordings in (**C**) (left); combined data (right). (**E**) Representative recordings of ipsilateral ITP-LN$_d$ and 5th s-LN$_v$ pair in *Clk856-Kir2.1* flies. (**F**) Cross-correlation analysis of recordings in (**E**) (left); combined data (right). (**G**) Combined frequencies of dual recordings in *WT*, *Clk856-TNT*, and *Clk856-Kir2.1* flies. n.s., not statistically significant difference by unpaired two-tailed Student's *t*-test. (**H**) Schematic of aMe ablation and dual recordings (top); representative neuronal excitability of ITP-LN$_d$ (middle) and 5th s-LN$_v$ (bottom) after aMe ablation. Similar results obtained in 5 independent replicates. Combined data are represented as means ± SEM.

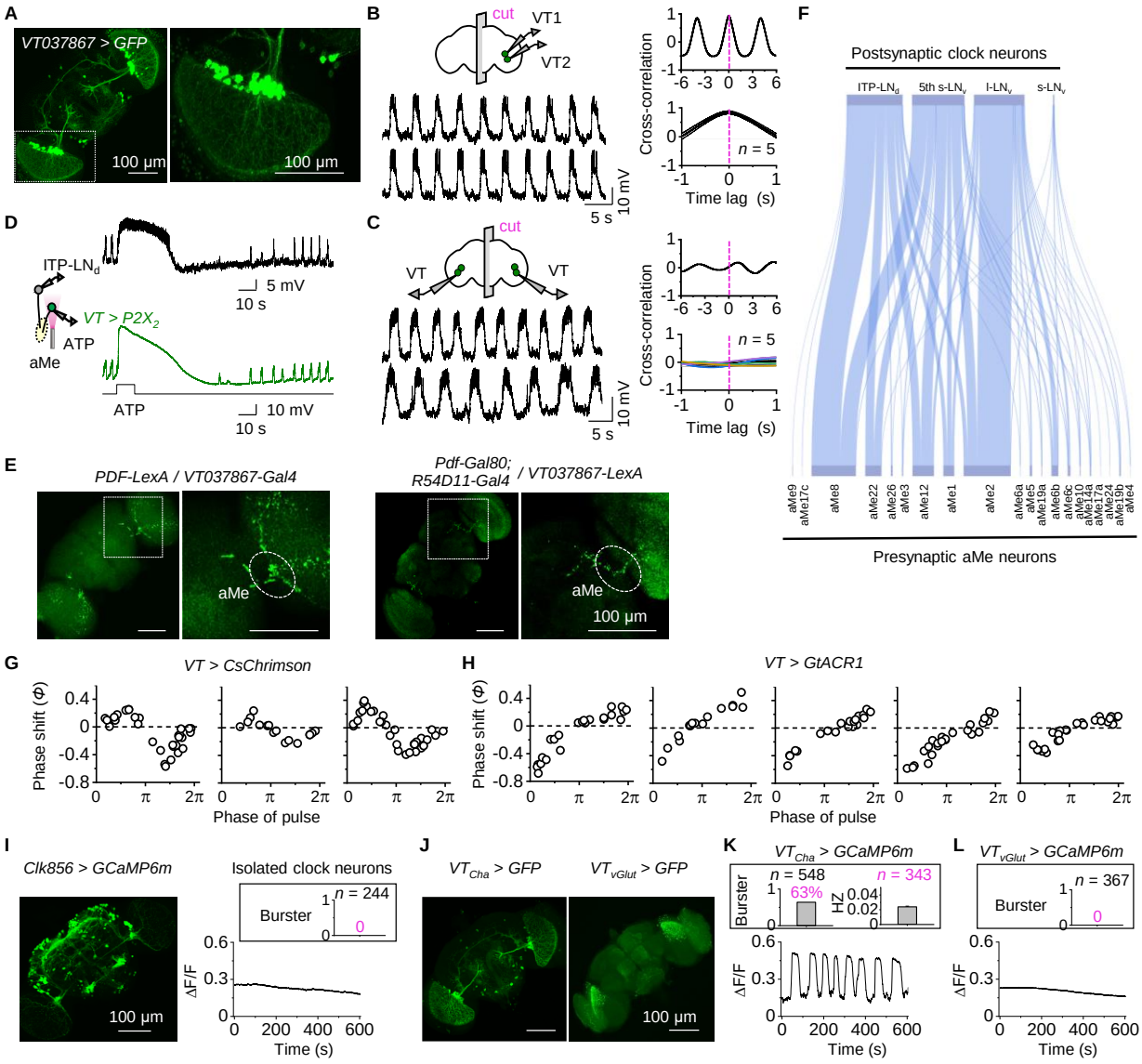

Fig. S3.

VT037867 neurons are *bona-fide* extra-clock ultradian electrical oscillators. (**A**) Left, neuronal labeling by *VT037867-Gal4*; right, expansion of the dashed rectangular on the left. (**B**) Representative recordings of ipsilateral pairs of VT037867 neurons in split brains (left), cross-correlation analysis (right). (**C**) Representative paired recordings from bilateral VT037867 neurons in split brains (left) and cross-correlation analysis (right). (**D**) Excitation of ITP-LN_d by 2.5 mM ATP-activation of $P2X_2$-expressing VT037867 neurons. Left, schematic of recordings of VT037867 and ITP-LN_d ipsilateral pairs; right, representative recordings. Similar results obtained in 9 independent replicates. (**E**) GRASP between VT037867 neurons and M cells and between VT037867 neurons and E cells. The dashed rectangular part on the left panel is expanded on the right. Similar results obtained in 6 independent replicates. (**F**) Synaptic connections between the VT037867-labeled aMe neurons and clock neurons based on the Hemibrain connectome dataset. The aMe neurons form 527, 495, 477, and 12 synapses with ITP-LN_d, 5th s-LN_v, l-LN_v, and s-LN_v, respectively. Among the aMe neurons, the aMe10, 12, and 26 form the dorsal commissure.

(**G**) The phase shift of VT037867 neurons by depolarization. (**H**) Phase shift of VT037867 neurons by hyperpolarization. (**I**) Left, clock neurons labeled by GCaMP6m with *Clk856-Gal4*; right, representative calcium-imaging trace of single isolated GCaMP6m-expressing clock neuron, with collective data shown in the inset. Combined results obtained in 6 independent replicates. (**J**) VT037867 subpopulations: ACh (left) and glutamate (right). (**K**) Calcium burst detected in ACh-expressing VT037867 neurons, with combined data in the inset. Combined data from 11 independent replicates. (**L**) No calcium burst was detected in glutamate-expressing VT037867 neurons, with combined data in the inset. Combined data from 6 independent replicates. Combined data are represented as means ± SEM.

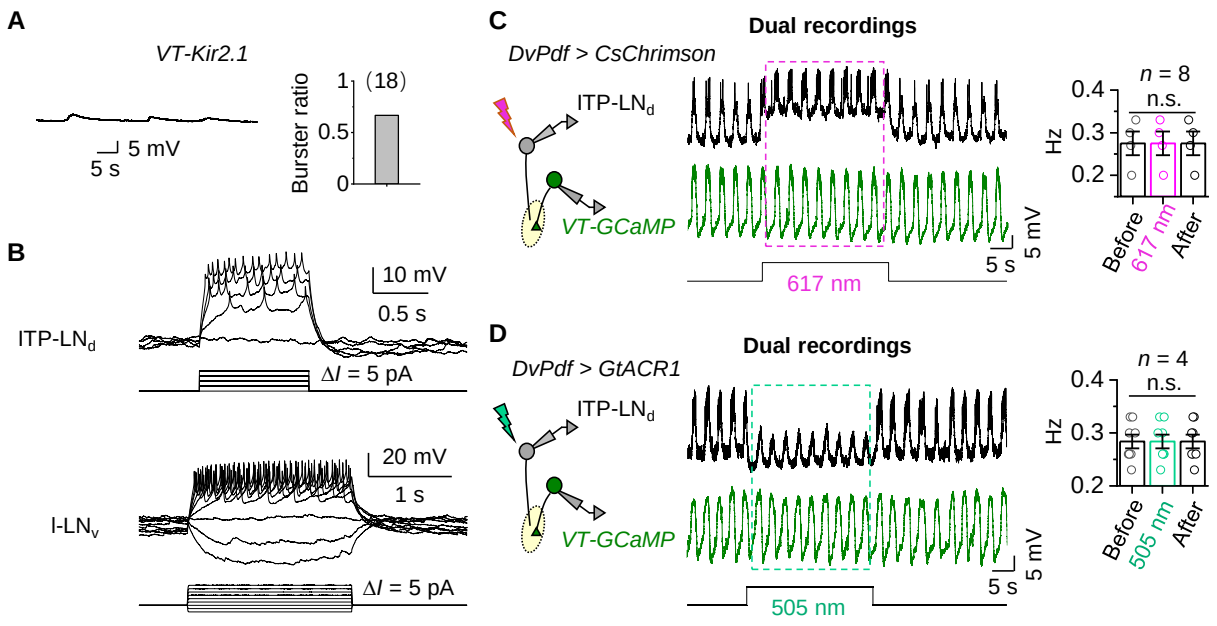

Fig. S4.

xCEOs drive ultradian bursting in clock neurons. (**A**) Weak oscillation of xCEOs in *VT037867-Kir2.1* flies. Left, representative small and slow oscillations; right, percentage of cells with subthreshold oscillations. (**B**) Excitability of clock neurons of *VT037867-Kir2.1* flies. Spike firing induced by current injection in ITP-LN_d (top) and l-LN_v (bottom). Similar results obtained in 12 and 8 independent replicates for ITP-LN_d and l-LN_v, respectively. (**C**) Left, schematic of recordings in *DvPdf-CsChrimson* flies; middle, representative dual recordings of xCEO and ITP-LN_d ipsilateral pair; right, combined data. Optogenetic stimulation: 617 nm, 30 s, 30 µW. n.s., not statistically significant difference by paired *t*-test. (**D**) Left, schematic of recordings in *DvPdf-GtACR1* flies; middle, representative dual recordings of xCEO and ITP-LN_d ipsilateral pair, right, combined data. Optogenetic stimulation: 505 nm, 30 s, 40 µW. n.s., no statistically significant difference by paired *t*-test. Combined data are represented as means ± SEM.

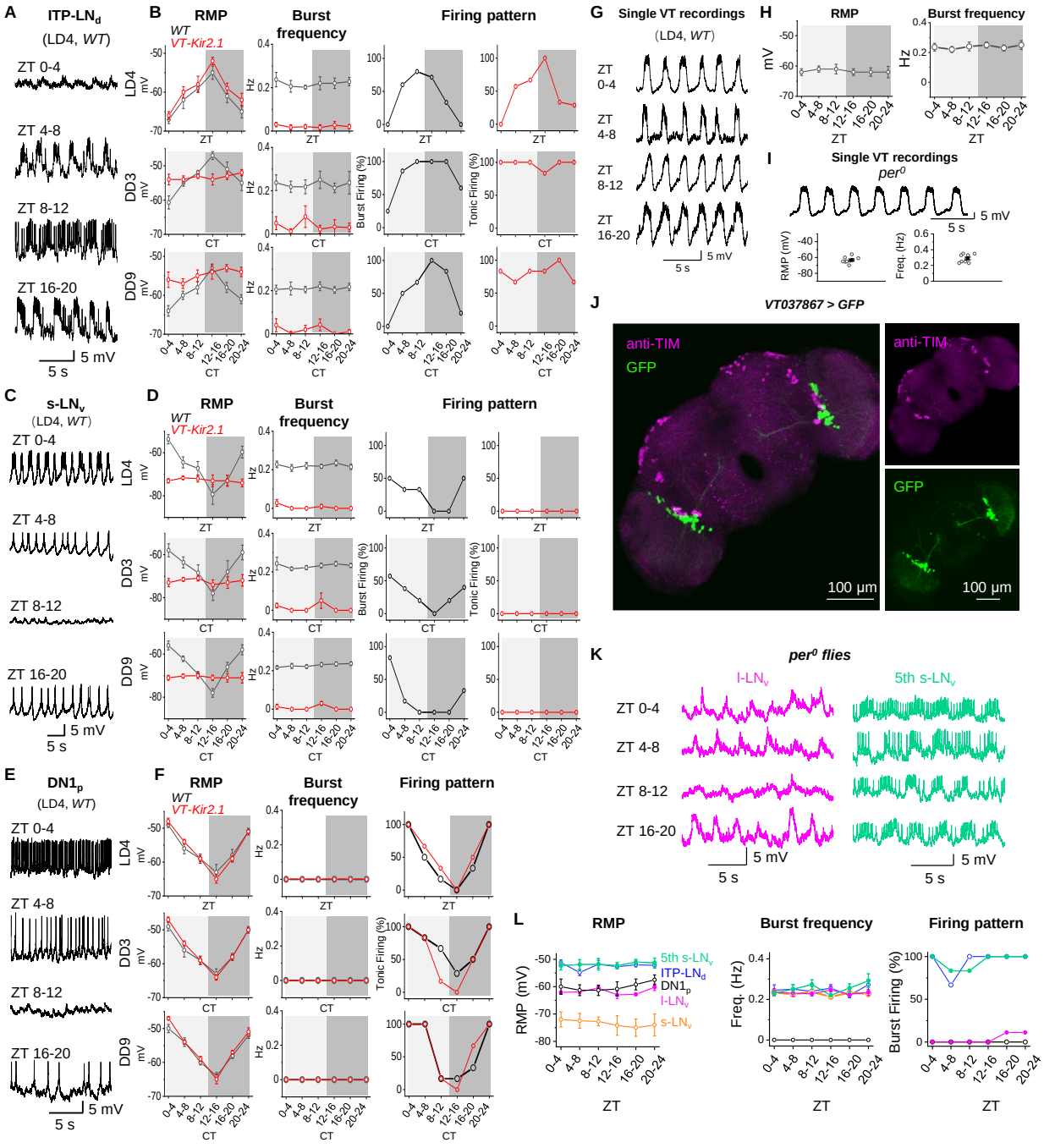

Fig. S5.

xCEOs promote daily electrical rhythms in clock neurons. (**A**) Representative current-clamp recordings (I = 0 pA) of ITP-LN$_d$ at different ZTs during LD4. (**B**) RMP rhythms (left), burst frequency (middle), and firing patterns (right) of ITP-LN$_d$ in *WT* and *VT037867-Kir2.1* flies. (**C**) Representative current-clamp recordings (I = 0 pA) of s-LN$_v$s at different ZTs during LD4. (**D**) RMP rhythms (left), burst frequency (middle), and firing patterns (right) of s-LN$_v$s in *WT* and *VT037867-Kir2.1* flies. (**E**) Representative current-clamp recordings (I = 0 pA) of DN1$_p$ at different ZTs during LD4. (**F**) RMP rhythms (left), burst frequency (middle), and firing patterns

(right) of $DN1_p$ in *WT* and *VT037867-Kir2.1* flies. (**G**) Representative current-clamp recordings (*I* = 0 pA) of xCEOs in *WT* flies at different ZTs during LD4. (**H**) Combined daily changes in RMPs and burst frequencies of xCEOs in *WT* flies. (**I**) bursts of xCEOs retained in per^0 flies (top) and combined RMPs and frequencies (bottom). (**J**) No clock gene expression in xCEOs. Immunostaining of TIM (magenta) and GFP (green) expressed in xCEOs. Similar results obtained in 5 independent replicates. (**K**) Representative daily activities of l-LN_v (left) and 5th s-LN_v (right) in per^0 flies at different ZTs during LD4. (**L**) Daily RMP rhythms (left), burst frequency (middle), and firing patterns (right) in s-LN_v, l-LN_v, ITP-LN_d, 5th s-LN_v, and $DN1_p$. ZT, zeitgeber time. CT, circadian time. Combined data are represented as means ± SEM. Each data point represents the average from 6 to 10 recorded cells.

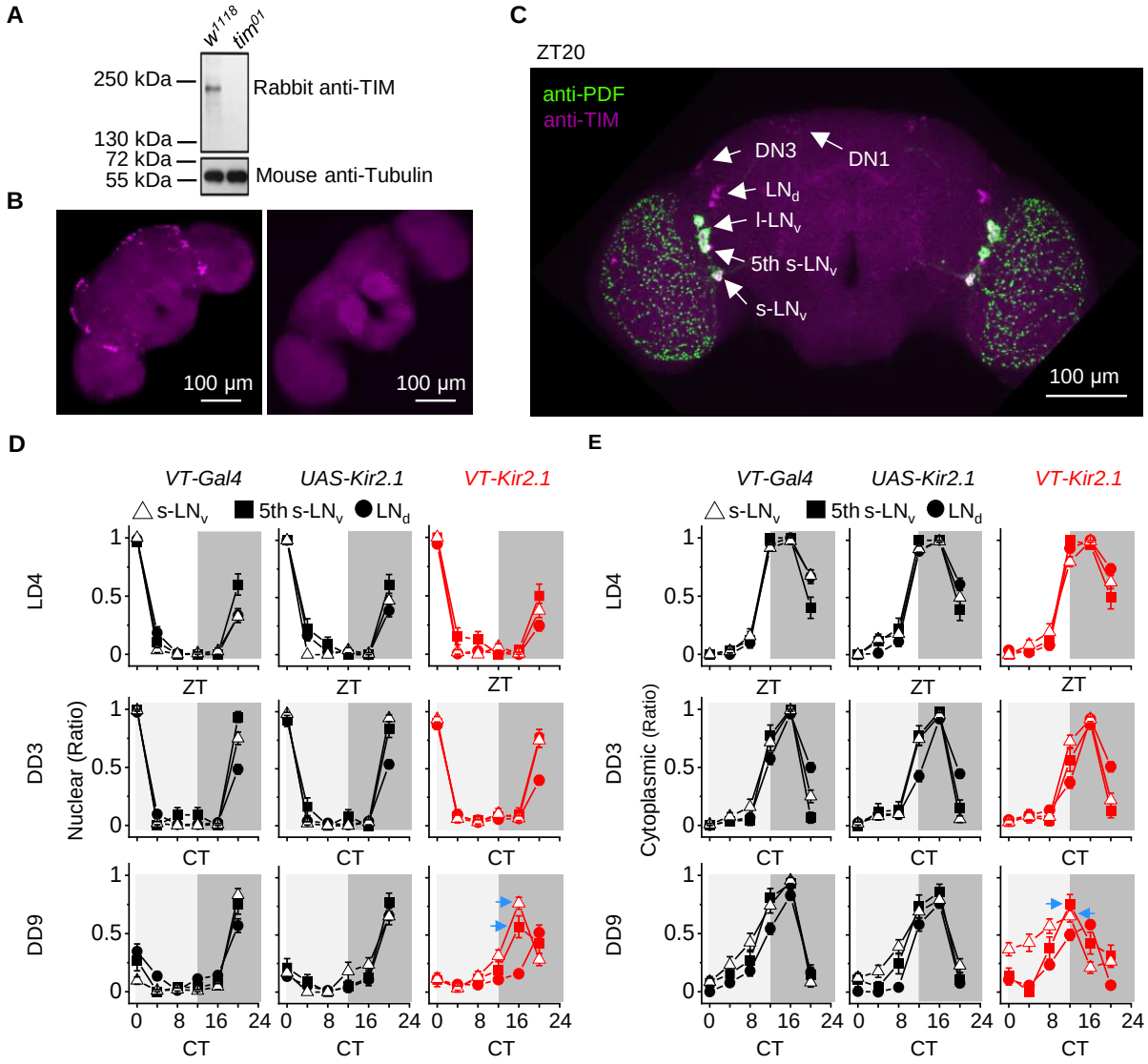

Fig. S6.

Validation of TIM antibody, and TIM subcellular distribution. (**A**) TIM expression in brain homogenates from w^{1118} and tim^{01} flies were analyzed by western blotting using TIM antibody. Similar results obtained in 4 independent replicates. (**B**) TIM expression in central clock neurons of w^{1118} (left) and tim^{01} (right) flies were analyzed by TIM antibody immunostaining. Similar results obtained in 4 independent replicates. (**C**) Immunostaining with anti-TIM (magenta) in *VT037867-Gal4* flies (ZT20, LD4). (**D**) Percentage of nuclear TIM distribution of s-LN_v, 5th s-LN_v, and LN_d in *VT037867-Gal4*, *UAS-Kir2.1*, and *VT037867-Kir2.1* flies. Slight phase desynchrony is indicated by blue arrows. (**E**) Percentage of cytoplasmic TIM distribution of s-LN_v, 5th s-LN_v, and LN_d in *VT037867-Gal4*, *UAS-Kir2.1*, *VT037867-Kir2.1* flies. ZT, zeitgeber time. CT, circadian time. Combined data are represented as means ± SEM. Immunostaining was independently repeated four times, with at least 25 brains examined in total at each time point.

Fig. S7.

Loss of DD locomotor rhythms in individual flies with xCEOs silenced in adults (*VT037867-Shibire^{ts}*). Adult-specific xCEO silencing induces DD arrhythmicity at 30 ℃, which re-establish rhythmicity at 18 ℃. Top, 28 individual arrhythmic flies at 30 ℃ in DD; bottom, 9 individual weak-rhythmic flies at 30 ℃ in DD.

Table S1.

Experiment genotypes used in this study.

Fig. 1A	*R18F07-p65.AD/+; R54D11-Gal4.DBD/UAS-mCD8-GFP* *R54D11-Gal4, UAS-mCD8-GFP*
Fig. 1B	*DvPdf-Gal4, UAS-mCD8-GFP* *UAS-mCD8-GFP; Clk4.1M-Gal4*
Fig. 1C	*R54D11-Gal4, UAS-mCD8-GFP* *DvPdf-Gal4, UAS-mCD8-GFP* *Mai179-Gal4, UAS-mCD8-GFP* *Clk856-Gal4, UAS-mCD8-GFP* *UAS-mCD8-GFP; Clk4.1M-Gal4*
Fig. 1D	*R54D11-Gal4, UAS-mCD8-GFP*
Fig. 1E	*R54D11-Gal4, UAS-mCD8-GFP*
Fig. 1F	*R54D11-Gal4, UAS-mCD8-GFP*
Fig. 1G	*R54D11-Gal4, UAS-mCD8-GFP*
Fig. 2A	per^{0}*/y; ; R54D11-Gal4, UAS-mCD8-GFP/+* (male) per^{S}*/y; ; R54D11-Gal4, UAS-mCD8-GFP/+* (male) per^{L}*/y; ; R54D11-Gal4, UAS-mCD8-GFP/+* (male) *DvPdf-Gal4, UAS-mCD8-GFP;* pdf^{01} *R54D11-Gal4, UAS-mCD8-GFP*
Fig. 2B	*UAS-TNT/Clk856-Gal4; DvPdf-LexA, LexAop2-GCaMP6m/+*
Fig. 2C	*R54D11-Gal4, UAS-mCD8-GFP*
Fig. 2D	*R54D11-Gal4, UAS-mCD8-GFP*
Fig. 2E	*R54D11-Gal4, UAS-mCD8-GFP*
Fig. 2F	*R54D11-Gal4, UAS-mCD8-GFP*
Fig. 2G	*R54D11-Gal4, UAS-mCD8-GFP*
Fig. 2H	*R54D11-Gal4, UAS-mCD8-GFP*
Fig. 3A	*UAS-mCD8-GFP; VT037867-Gal4* *+/+; VT037867-Gal4/UAS-syt.eGFP*
Fig. 3B	*UAS-mCD8-GFP; VT037867-Gal4*
Fig. 3C	*UAS-mCD8-GFP; VT037867-Gal4*
Fig. 3D	*UAS-mCD8-GFP/+; VT037867-Gal4/R54D11-Gal4, UAS-mCD8-GFP*
Fig. 3E	*UAS-CsChrimson/+; DvPdf-LexA, LexAop2-GCaMP6m/VT037867-Gal4*
Fig. 3F	*UAS-CsChrimson/+; DvPdf-LexA, LexAop2-GCaMP6m/VT037867-Gal4*
Fig. 3G	*UAS-GtACR1/+; DvPdf-LexA, LexAop2-GCaMP6m/VT037867-Gal4*
Fig. 3H	*UAS-GCaMP6m; VT037867-Gal4, UAS-GCaMP6m*
Fig. 3I	*UAS-GCaMP6m; VT037867-Gal4, UAS-GCaMP6m*
Fig. 4A	*UAS-mCD8-GFP; VT037867-Gal4* *UAS-Kir2.1; VT037867-Gal4, UAS-GCaMP6m*
Fig. 4B	*UAS-mCD8-GFP; VT037867-Gal4* *UAS-Kir2.1; VT037867-Gal4, UAS-GCaMP6m*
Fig. 4C	*UAS-Kir2.1/+; DvPdf-LexA, LexAop2-GCaMP6m/VT037867-Gal4* *UAS-Kir2.1/Pdf-LexA, LexAop2-GFP; VT037867-Gal4/+*
Fig. 4D	*UAS-Kir2.1/+; DvPdf-LexA, LexAop2-GCaMP6m/VT037867-Gal4*

	UAS-Kir2.1/Pdf-LexA, LexAop2-GFP; VT037867-Gal4/+ *UAS-Kir2.1/+; DvPdf-LexA, LexAop2-GCaMP6m/+* *UAS-Kir2.1/Pdf-LexA, LexAop2-GFP; +/+*
Fig. 4E	*UAS-GtACR1/+; DvPdf-LexA, LexAop2-GCaMP6m/VT037867-Gal4*
Fig. 4F	*UAS-GtACR1/+; DvPdf-LexA, LexAop2-GCaMP6m/VT037867-Gal4*
Fig. 4G	*UAS-CsChrimson/+; DvPdf-LexA, LexAop2-GCaMP6m/VT037867-Gal4*
Fig. 4H	*UAS-CsChrimson/+; DvPdf-LexA, LexAop2-GCaMP6m/VT037867-Gal4*
Fig. 4I	*UAS-CsChrimson/+; DvPdf-LexA, LexAop2-GCaMP6m/VT037867-Gal4*
Fig. 4J	*UAS-GtACR1/+; DvPdf-LexA, LexAop2-GCaMP6m/VT037867-Gal4*
Fig. 5A	*UAS-Kir2.1/Pdf-LexA,LexAop2-GFP; +/+* *UAS-Kir2.1/Pdf-LexA, LexAop2-GFP; VT037867-Gal4/+*
Fig. 5B	*UAS-Kir2.1/+; DvPdf-LexA, LexAop2-GCaMP6m/+* *UAS-Kir2.1/+; DvPdf-LexA, LexAop2-GCaMP6m/VT037867-Gal4*
Fig. 5C	*UAS-Kir2.1/Pdf-LexA,LexAop2-GFP; +/+* *UAS-Kir2.1/Pdf-LexA,LexAop2-GFP; VT037867-Gal4/+* *UAS-Kir2.1/+; DvPdf-LexA, LexAop2-GCaMP6m/+* *UAS-Kir2.1/+; DvPdf-LexA, LexAop2-GCaMP6m/VT037867-Gal4*
Fig. 5D	*UAS-Kir2.1/Pdf-LexA,LexAop2-GFP; +/+* *UAS-Kir2.1/Pdf-LexA,LexAop2-GFP; VT037867-Gal4/+* *UAS-Kir2.1/+; DvPdf-LexA, LexAop2-GCaMP6m/+* *UAS-Kir2.1/+; DvPdf-LexA, LexAop2-GCaMP6m/VT037867-Gal4*
Fig. 5E	*UAS-Kir2.1/Pdf-LexA,LexAop2-GFP; +/+* *UAS-Kir2.1/Pdf-LexA,LexAop2-GFP; VT037867-Gal4/+* *UAS-Kir2.1/+; DvPdf-LexA, LexAop2-GCaMP6m/+* *UAS-Kir2.1/+; DvPdf-LexA, LexAop2-GCaMP6m/VT037867-Gal4*
Fig. 6A	*VT037867-Gal4* *UAS-Kir2.1; VT037867-Gal4,UAS-Kir2.1-GFP/ VT037867-Gal4*
Fig. 6B	*VT037867-Gal4* *UAS-Kir2.1* *UAS-Kir2.1; VT037867-Gal4,UAS-Kir2.1-GFP/ VT037867-Gal4*
Fig. 6C	*VT037867-Gal4* *UAS-Kir2.1* *UAS-Kir2.1; VT037867-Gal4,UAS-Kir2.1-GFP/ VT037867-Gal4*
Fig. 6D	*VT037867-Gal4* *UAS-Kir2.1* *UAS-Kir2.1; VT037867-Gal4,UAS-Kir2.1-GFP/ VT037867-Gal4*
Fig. 7A	*VT037867-Gal4* *UAS-Kir2.1* *UAS-Kir2.1; VT037867-Gal4*
Fig. 7B	*UAS-Kir2.1; VT037867-Gal4*
Fig. 7C	*UAS-Shibire^{ts}; VT037867-Gal4,UAS-Shibire^{ts}*
Fig. 7D	*VT037867-Gal4* *UAS-Kir2.1* *UAS-Kir2.1; VT037867-Gal4* *UAS-Shibire^{ts}; VT037867-Gal4,UAS-Shibire^{ts}*
Fig. 7E	*VT037867-Gal4*

	UAS-Kir2.1 *UAS-Kir2.1; VT037867-Gal4* *UAS-Shibire^{ts}; VT037867-Gal4,UAS-Shibire^{ts}*
Fig. S1A	*R54D11-Gal4, UAS-mCD8-GFP*
Fig. S1B	*R54D11-Gal4, UAS-mCD8-GFP*
Fig. S1C	*DvPdf-Gal4, UAS-mCD8-GFP*
Fig. S1D	*DvPdf-Gal4, UAS-mCD8-GFP*
Fig. S1E	*R54D11-Gal4, UAS-mCD8-GFP*
Fig. S1F	*R54D11-Gal4, UAS-mCD8-GFP*
Fig. S1G	*R54D11-Gal4, UAS-mCD8-GFP*
Fig. S1H	*R54D11-Gal4, UAS-mCD8-GFP*
Fig. S2A	*UAS-TNT/Clk856-Gal4; DvPdf-LexA, LexAop2-GCaMP6m/+*
Fig. S2B	*UAS-TNT/Clk856-Gal4; DvPdf-LexA, LexAop2-GCaMP6m/+*
Fig. S2C	*UAS-TNT/Clk856-Gal4; DvPdf-LexA, LexAop2-GCaMP6m/+*
Fig. S2D	*UAS-TNT/Clk856-Gal4; DvPdf-LexA, LexAop2-GCaMP6m/+*
Fig. S2E	*UAS-Kir2.1/Clk856-Gal4; DvPdf-LexA, LexAop2-GCaMP6m/+*
Fig. S2F	*UAS-Kir2.1/Clk856-Gal4; DvPdf-LexA, LexAop2-GCaMP6m/+*
Fig. S2G	*UAS-TNT/Clk856-Gal4; DvPdf-LexA, LexAop2-GCaMP6m/+* *UAS-Kir2.1/Clk856-Gal4; DvPdf-LexA, LexAop2-GCaMP6m/+* *DvPdf-Gal4, UAS-mCD8-GFP*
Fig. S2H	*R54D11-Gal4, UAS-mCD8-GFP*
Fig. S3A	*UAS-mCD8-GFP; VT037867-Gal4*
Fig. S3B	*UAS-mCD8-GFP; VT037867-Gal4*
Fig. S3C	*UAS-mCD8-GFP; VT037867-Gal4*
Fig. S3D	*DvPdf-LexA, LexAop2-GCaMP6f/+; UAS-GCaMP6m,UAS-P2X$_2$/VT037867-Gal4*
Fig. S3E	*Pdf-LexA/+; VT037867-Gal4/UAS-mCD4::spGFP$^{1-10}$,LexAop-mCD4::GFP^{11}* *VT037867-LexA/Pdf-Gal80; R54D11-Gal4/UAS-mCD4::spGFP$^{1-10}$,LexAop-mCD4::GFP^{11}*
Fig. S3G	*UAS-CsChrimson/+; DvPdf-LexA, LexAop2-GCaMP6m/VT037867-Gal4*
Fig. S3H	*UAS-GtACR1/+; DvPdf-LexA, LexAop2-GCaMP6m/VT037867-Gal4*
Fig. S3I	*Clk856-Gal4, UAS-GCaMP6m*
Fig. S3J	*UAS-FRT-Stop-FRT-GFP/+; VT037867-Gal4, Cha-Flp/+* *UAS-FRT-Stop-FRT-GFP/vGlut-Flp; VT037867-Gal4/+*
Fig. S3K	*UAS-FRT-Stop-FRT-GCaMP6m/+; VT037867-Gal4, Cha-Flp/+*
Fig. S3L	*vGlut-p65.AD/UAS-GCaMP6m; VT037867-Gal4.DBD/+*
Fig. S4A	*UAS-Kir2.1; VT037867-Gal4, UAS-GCaMP6m*
Fig. S4B	*UAS-Kir2.1/+; DvPdf-LexA, LexAop2-GCaMP6m/VT037867-Gal4* *UAS-Kir2.1/Pdf-LexA, LexAop2-GFP; VT037867-Gal4/+*
Fig. S4C	*LexAop2-CsChrimson/+; DvPdf-LexA,LexAop2-GCaMP6m/VT037867-Gal4,UAS-GCaMP6m*
Fig. S4D	*LexAop2-GtACR1/+; DvPdf-LexA,LexAop2-GCaMP6m/VT037867-Gal4,UAS-GCaMP6m*
Fig. S5A	*UAS-Kir2.1/+; DvPdf-LexA, LexAop2-GCaMP6m/+*
Fig. S5B	*UAS-Kir2.1/+; DvPdf-LexA, LexAop2-GCaMP6m/+*

	UAS-Kir2.1/+; DvPdf-LexA, LexAop2-GCaMP6m/VT037867-Gal4
Fig. S5C	*UAS-Kir2.1/Pdf-LexA,LexAop2-GFP; +/+*
Fig. S5D	*UAS-Kir2.1/Pdf-LexA,LexAop2-GFP; +/+* *UAS-Kir2.1/Pdf-LexA,LexAop2-GFP; VT037867-Gal4/+*
Fig. S5E	*UAS-Kir2.1/+; Clk4.1M-LexA,LexAop2-GCaMP6m/+*
Fig. S5F	*UAS-Kir2.1/+; Clk4.1M-LexA,LexAop2-GCaMP6m/+* *UAS-Kir2.1/+; Clk4.1M-LexA,LexAop2-GCaMP6m/VT037867-Gal4*
Fig. S5G	*UAS-mCD8-GFP; VT037867-Gal4*
Fig. S5H	*UAS-mCD8-GFP; VT037867-Gal4*
Fig. S5I	per^0*/y; UAS-mCD8-GFP/+; VT037867-Gal4/+* (male)
Fig. S5J	*UAS-mCD8-GFP; VT037867-Gal4*
Fig. S5K	per^0*/y; Pdf-LexA,LexAop2-GFP/+; +/+* (male) per^0*/y; DvPdf-Gal4, UAS-mCD8-GFP/+; +/+* (male)
Fig. S5L	per^0*/y; Pdf-LexA,LexAop2-GFP/+; +/+ (male)* per^0*/y; DvPdf-Gal4, UAS-mCD8-GFP/+; +/+* (male) per^0*/y; ; Clk4.1M-LexA,LexAop2-GCaMP6m/+* (male)
Fig. S6A	w^{1118} tim^{01}
Fig. S6B	w^{1118} tim^{01}
Fig. S6C	*VT037867-Gal4*
Fig. S6D	*VT037867-Gal4* *UAS-Kir2.1* *UAS-Kir2.1; VT037867-Gal4,UAS-Kir2.1-GFP/ VT037867-Gal4*
Fig. S6E	*VT037867-Gal4* *UAS-Kir2.1* *UAS-Kir2.1; VT037867-Gal4,UAS-Kir2.1-GFP/ VT037867-Gal4*
Fig. S7	*UAS-Shibire^{ts}; VT037867-Gal4,UAS-Shibire^{ts}*

Movie S1. Cell-autonomous ultradian oscillation in single VT037867 neurons.

A single dissociated GCaMP6m-expressing VT037867 neuron exhibited cell-autonomous ultradian rhythmic calcium oscillations (left) and the plot of real-time fluorescence changes (right).